Instabilities of one-dimensional stationary solutions of the cubic nonlinear Schrödinger equation

Draft - August 27, 2005

Abstract

We consider the two-dimensional cubic nonlinear Schrödinger (NLS) equation, which admits a large family of one-dimensional bounded traveling-wave solutions. All such stationary solutions may be written in terms of an amplitude and a phase. Solutions with piecewise constant phase have been well studied [18, 16, 15, 10, 4], and no stable stationary solutions exist. Here we consider stability of the larger class of solutions whose phase is dependent on the spatial dimension of the one-dimensional wave form. These solutions are said to have nontrivial-phase (NTP). We study the spectral stability of such NTP solutions numerically, using (a spectrally based) Hill's method. We present evidence which suggests that all such NTP solutions are unstable with respect to both one-dimensional and transverse perturbations. Instability occurs in all cases: for both the elliptic and hyperbolic NLS equations, and in the focusing and defocusing case.

1 Introduction

The cubic nonlinear Schrödinger (NLS) equation in two spatial dimensions is given by

$$i\psi_t + \alpha\psi_{xx} + \beta\psi_{yy} + |\psi|^2\psi = 0. \tag{1}$$

The NLS equation is said be *focusing* or *attractive* in the x-dimension if $\alpha > 0$. If $\alpha < 0$, NLS is said to be *defocusing* or *repulsive* in the x-dimension. Similarly, the sign of β leads to focusing or defocusing in the y-dimension [17]. The NLS equation is called *hyperbolic* if $\alpha\beta < 0$ and *elliptic* if $\alpha\beta > 0$. Without loss of generality, both α and β are chosen to be ± 1.

Equation (1) admits a large family of one-dimensional bounded traveling-wave solutions. All such solutions, modulo Lie group symmetries, may be written in the form [17]

$$\psi(x,t) = \phi(x)e^{i\theta(x)+i\lambda t}, \tag{2}$$

where $\phi(x)$ and $\theta(x)$ are real-valued functions, and λ is a real constant. Solutions of the form (2) are possible if

$$\phi^2(x) = \alpha\left(-2k^2\,\mathrm{sn}^2(x,k) + B\right), \tag{3a}$$

$$\theta(x) = c\int_0^x \phi^{-2}(\xi)d\xi, \tag{3b}$$

$$\lambda = \frac{1}{2}\alpha(3B - 2(1+k^2)), \tag{3c}$$

$$c^2 = -\frac{\alpha^2}{2}B(B-2k^2)(B-2), \tag{3d}$$

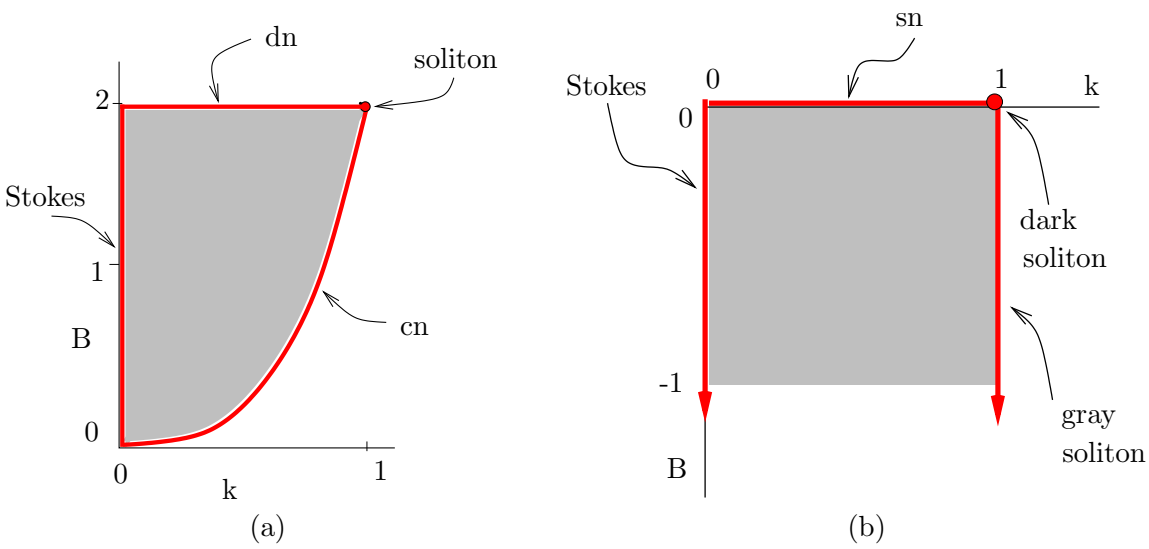

Figure 1: Admissible parameter space for solutions of the form given in (2) for (a) focusing ($\alpha = 1$) and (b) defocusing ($\alpha = -1$) regimes. The gray interior region corresponds to NTP solutions.

where c is a real constant. Here $k \in [0, 1]$ is the elliptic modulus of the Jacobi elliptic sine function, $\mathrm{sn}\,(x, k)$. The function $\mathrm{sn}\,(x, k)$ is periodic if $k \in [0, 1)$, with period given by $L = 4K$, where $K = K(k)$ is defined by

$$K(k) = \int_0^{\pi/2} \left(1 - k^2 \sin^2 x\right)^{-1/2} dx, \tag{4}$$

which is the complete elliptic integral of the first kind. When $k = 0$, $\mathrm{sn}\,(x, 0) = \sin(x)$ with $L = 2\pi$. As k approaches 1, $\mathrm{sn}\,(x, k)$ limits to $\tanh(x)$ and L approaches infinity [2].

The solution ψ is said to have *trivial-phase* (TP) if $\theta(x)$ is (piecewise) constant and *nontrivial-phase* (NTP) if $\theta(x)$ is not constant. Equivalently, the solution ψ has TP if $c = 0$, and has NTP if $c \neq 0$. For every choice of α and β, (3) specifies a two-parameter family of solutions in the free parameters k and B. Without loss of generality, both α and β are chosen to be ± 1. The phase contribution $\theta(x)$ of (3b) implicitly depends on α and B in both (3a) and (3d). In order for ϕ and θ to be real-valued functions, we need $B \in [2k^2, 2]$ if $\alpha = 1$ or $B \leq 0$ if $\alpha = -1$. Figure 1 represents the (k, B)-parameter space corresponding to NTP solutions of the NLS equation. As $c \to 0$, the phase θ approaches a (piecewise) constant, and the NTP solutions reduce to one of five simpler types of TP solutions: (*i*) a Stokes' plane wave, (*ii*) a cn-type solution, (*iii*) a dn-type solution, (*iv*) an sn-type solution, (*v*) a soliton-type solution. The limiting solutions correspond to the boundaries of the regions in Fig. 1. Table 1 provides the values of k and B that cause (2) to limit to the simpler solutions, and also gives the explicit expression of ψ for all but one. A cumbersome expression in the case of the gray soliton has been omitted. An overview of these NLS solutions is given in [3]. Details of the Jacobi elliptic functions sn, cn and dn may be found in [2].

While both TP and NTP solutions are of interest, stability of TP solutions is well understood: for example, see see [18, 14, 13, 8, 16, 15, 7, 4]. All TP solutions are known to be unstable, see /citeJCBDtp and the references therein We know of only Infeld and Ziemkiewicz's paper [10] which considers the stability of NTP solutions of the NLS equation. The (k, B)-parameter space

$i\alpha = 1$	$k = 0$	$B \in [2k^2, 2]$	Stokes' plane wave	$\sqrt{B}\, e^{i(qx+\lambda t)}$
	$k \in (0,1)$	$B = 2k^2$	cn-type	$\sqrt{2}\ \mathrm{cn}\,(x,k)\, e^{i(2k^2-1)t}$
	$k \in (0,1)$	$B = 2$	dn-type	$\sqrt{2}\ \mathrm{dn}\,(x,k)\, e^{i(2-k^2)t}$
	$k = 1$	$B = 2$	bright soliton	$\sqrt{2}\ \mathrm{sech}(x) e^{it}$
$\alpha = -1$	$k = 0$	$B \leq 0$	Stokes' plane wave	$\sqrt{B}\, e^{i(qx+\lambda t)}$
	$k \in (0,1)$	$B = 0$	sn-type	$\sqrt{2}\ \mathrm{sn}\,(x,k) e^{i(1+k^2)t}$
	$k = 1$	$B = 0$	dark soliton	$\sqrt{2}\ \tanh(x)\, e^{i2t}$
	$k = 1$	$B < 0$	gray soliton	not incl.

Table 1: Parameter values (k, B) which reduce the NTP solution form (2) to simpler TP solutions. Here q is an arbitrary wavenumber.

of TP solutions is essentially one-dimensional; it forms the boundary of the NTP parameter spaces shown in Fig. 1. The dimension of the NTP solution space is fully two dimensional. We had hoped that this much larger parameter space would yield NTP solutions that would be stable under one-dimensional and/or transverse perturbations. The more difficult linear stability problem and the large parameter space that needs to be explored makes the NTP setting more complex than the TP setting. In this paper, we investigate the spectral stability of all NTP solutions (2), for all choices of $\alpha = \pm 1$ and $\beta = \pm 1$. That is, we compute the eigenvalues of an approximate spectral problem in order to identify possible growing modes in the linear stability problem. A similar treatment of all TP solutions is found in [4]. No spectrally stable NTP solutions were found, but the search did provide important stability information.

2 The linear stability problem

In order to study the linear stability of NTP solutions of the NLS equation, we consider perturbations of the form

$$\psi_p(x,y,t) = (\phi(x) + \epsilon u(x,y,t) + i\epsilon v(x,y,t) + \mathcal{O}(\epsilon^2))\mathrm{e}^{i\theta(x)+i\lambda t}, \tag{5}$$

where $u(x,y,t)$ and $v(x,y,t)$ are real-valued functions, ϵ is a small real parameter and $\phi(x)\mathrm{e}^{i\theta(x)+i\lambda t}$ is a NTP solution of NLS. Substituting (5) in (1), linearizing and separating real and imaginary parts leads to

$$\lambda u - 3\gamma\phi^2 u - \beta u_{yy} + \alpha c^2 \frac{1}{\phi^4} u - 2\alpha c \frac{1}{\phi^3}\phi_x v + 2\alpha c \frac{1}{\phi^2} v_x - \alpha u_{xx} = -v_t, \tag{6a}$$

$$\lambda v - \gamma\phi^2 v - \beta v_{yy} + \alpha c^2 \frac{1}{\phi^4} v + 2\alpha c \frac{1}{\phi^3}\phi_x u - 2\alpha c \frac{1}{\phi^2} u_x - \alpha v_{xx} = u_t. \tag{6b}$$

Since (6) does not depend on y or t explicitly, we may assume that $u(x,y,t)$ and $v(x,y,t)$ have the form

$$u(x,y,t) = U(x,\rho,\Omega)\mathrm{e}^{i\rho y+\Omega t} + c.c., \tag{7a}$$

$$v(x,y,t) = V(x,\rho,\Omega)\mathrm{e}^{i\rho y+\Omega t} + c.c., \tag{7b}$$

where ρ is a real constant, $U(x)$ and $V(x)$ are complex-valued functions, Ω is a complex constant and *c.c.* denotes complex conjugate. Notice that ρ is the wavenumber of the transverse perturbation and Ω is the exponential growth rate associated with ρ. If bounded U, V exist such that Ω has a positive real part, then the amplitudes of the perturbations grow exponentially in time and the unperturbed solution is said to be unstable.

Upon substitution, (6) gives

$$\lambda U - 3\gamma\phi^2 U + \beta\rho^2 U + \alpha c^2 \frac{1}{\phi^4} U - 2\alpha c \frac{1}{\phi^3}\phi_x V + 2\alpha c \frac{1}{\phi^2} V_x - \alpha U_{xx} = -\Omega V, \tag{8a}$$

$$\lambda V - \gamma\phi^2 V + \beta\rho^2 V + \alpha c^2 \frac{1}{\phi^4} V + 2\alpha c \frac{1}{\phi^3}\phi_x U - 2\alpha c \frac{1}{\phi^2} U_x - \alpha V_{xx} = \Omega U. \tag{8b}$$

If $c = 0$, then (8) reduces to the stability analysis of TP solutions. This case is examined in [5, 4, 10, 1, 12, 15] and others. Using the linear system (8), we are now able to investigate the stability of the perturbed NTP solution numerically.

3 Numerical investigation of spectral stability

The main difficulty for the numerical investigation of (8) is the size of the parameter space involved. For every choice of the equations parameters α, β and solution parameter pairs (k, B), the spectrum of (8) needs to computed for a range of ρ values to determine stability or to analyze any instabilities. An efficient numerical method is necessary. Hill's method [6], which exhibits exponential convergence, allows for the systematic exploration of the large phase space encountered here.

3.1 Hill's method

To apply Hill's method, Fourier expansions are needed for all coefficients of (8). Using the complex Fourier form, we have

$$\begin{aligned} \phi^2(x) &= \sum_{n=-\infty}^{\infty} Q_n e^{i2n\pi x/L}, & \phi^{-2}(x) &= \sum_{n=-\infty}^{\infty} R_n e^{i2n\pi x/L}, \\ \phi^{-4}(x) &= \sum_{n=-\infty}^{\infty} S_n e^{i2n\pi x/L}, & \phi^{-3}(x)\phi'(x) &= \sum_{n=-\infty}^{\infty} T_n e^{i2n\pi x/L}, \end{aligned} \tag{9}$$

where Q_n, R_n, S_n and T_n are the Fourier coefficients. We note that $\phi^2(x)$ has period $L/2$ and that $\phi(x)$ is never zero except in the TP limit cases.

The periodicity of the coefficients in (8) allows us to decompose the eigenfunction components U and V of the spectral problem in a Fourier-Floquet form

$$U(x) = e^{i\mu x} \sum_{n=-\infty}^{\infty} U_n e^{-in\pi x/L} \quad \text{and} \quad V(x) = e^{i\mu x} \sum_{n=-\infty}^{\infty} V_n e^{-in\pi x/L}. \tag{10}$$

The form of U and V in (10) follows from Floquet's theorem and the observation that we seek eigenfunctions, which are by definition bounded. This decomposition has the benefit of admitting both periodic and anti-periodic eigenfunctions when $\mu = 0$. Allowing the Floquet exponent μ to

be different from 0 gives rise to solutions that are either quasiperiodic or have period greater than L. Again, see [6] for a more complete explanation and discussion.

Substitution of (9) and (10) in (8) and equating Fourier coefficients allows us to write equations for U_n and V_n as a coupled bi-infinite system of difference equations given by

$$-\left(\lambda+\beta\rho^2-\alpha\left(i\mu+\frac{in\pi}{L}\right)^2\right)U_n+3\gamma\sum_{m=-\infty}^{\infty}Q_{\frac{n-m}{2}}U_m-\alpha c^2\sum_{m=-\infty}^{\infty}S_{\frac{n-m}{2}}U_m$$
$$+2\alpha c\sum_{m=-\infty}^{\infty}T_{\frac{n-m}{2}}V_m-2\alpha c\left(i\mu+\frac{in\pi}{L}\right)\sum_{m=-\infty}^{\infty}R_{\frac{n-m}{2}}V_m=\Omega V_n \quad (11a)$$

$$\left(\lambda+\beta\rho^2-\alpha\left(i\mu+\frac{in\pi}{L}\right)^2\right)V_n-\gamma\sum_{m=-\infty}^{\infty}Q_{\frac{n-m}{2}}V_m+\alpha c^2\sum_{m=-\infty}^{\infty}S_{\frac{n-m}{2}}V_m$$
$$+2\alpha c\sum_{m=-\infty}^{\infty}T_{\frac{n-m}{2}}U_m-2\alpha c\left(i\mu+\frac{in\pi}{L}\right)\sum_{m=-\infty}^{\infty}R_{\frac{n-m}{2}}U_m=\Omega U_n. \quad (11b)$$

The system of equations (11a) and (11b) is *equivalent* to the original system (8), and holds for all integers n. Here $\mu\in[\frac{-\pi}{K},\frac{\pi}{K})$ and $Q_{\frac{n-m}{2}}=0$ if $n-m\notin 2\mathbb{Z}$, with $R_{(\cdot)},S_{(\cdot)}$ and $T_{(\cdot)}$ similarly defined.

In practice, a pre-multiplication of the linear system by ϕ^4 allows for an exact cosine series expansion of ϕ^2,ϕ^4 and ϕ^6 to be used. This follows from the differential equations for $\mathrm{sn}\,(x,k)$ and Jacobi's [11] series expansion of $\mathrm{sn}^2(x,k)$. This pre-multiplication transforms the original eigenvalue problem into a generalized eigenvalue problem. Golub and Van Loan [9] provide a brief discussion of generalized eigenvalue problems.

3.2 Numerical Experiments

By choosing a finite number of Fourier modes, thus truncating the exact bi-infinite system (11), we explicitly construct and compute approximations to the spectral elements of (8). We consider all four cases: (I) focusing in both x and y ($\alpha=\beta=1$), (II) focusing in x and defocusing in y ($\alpha=-\beta=1$), (III) defocusing in x and focusing in y ($-\alpha=\beta=1$) and finally, (IV) defocusing in both x and y ($-\alpha=-\beta=1$).

In each case, a large number of parameter values in the two-dimensional parameter space shown in Fig. 1 was explored numerically. Approximately 5.2 million generalized eigenvalue problems were considered, the size of each determined by the cutoff mode N of the underlying Fourier series. A truncation to N Fourier modes reduces the bi-infinite exact system (11) to an approximate $(4N+2)$-dimensional problem. For several choices of k and B, a value of $N=N(k,B)$ was chosen to ensure that the resulting eigenvalues had converged to within a measured tolerance. A simple polynomial was used to fit this data. This information, and details related to other parameter ranges used in the experiments, are included in Table 2. In the table, k is the elliptic modulus, B is the offset parameter and may be interpreted as a measure of the nontrivial-phase quantity θ, $(4N+2)$ is the matrix dimension used to approximate the full operator, ρ is the wavenumber of the perturbation in the y-dimension, and μ is the Floquet exponent. Lastly, `linspace(a,b,m)` is a linearly spaced vector from a to b of length m, `logspace(a,b,m)` is a logarithmically spaced vector from 10^a to 10^b of length m and function `ceil(x)` is the smallest integer not less than x.

Parameter	Description	Value
k	Elliptic modulus	$\texttt{linspace(0,1,65)}$
B	Shift	For $\alpha = -1$: $-\texttt{logspace}(-8,0,65)$ For $\alpha = \ \ 1$: $(2k^2 + \texttt{logspace}(-8,0,65)) \cap (2k^2, 2)$
N	Fourier cutoff	For $\alpha = -1$: $15 + \texttt{ceil}(5\texttt{k}^5)$ For $\alpha = \ \ 1$: $10 + \texttt{ceil}(25\texttt{k}^{10})$
ρ	Perturbation wavenumber	$\texttt{linspace(0,4,65)}$
μ	Floquet parameter	$\texttt{linspace}(-\frac{\pi}{\texttt{K}}, \frac{\pi}{\texttt{K}}, 21)$

Table 2: Parameter values and ranges used in numerical experiments.

3.3 Observations

First and foremost, it should be stated that *none* of the solutions considered here were found to be spectrally stable under one-dimensional and transverse perturbations. This establishes, at least numerically, that *all* one-dimensional traveling-wave solutions of NLS of the form given by (2) are spectrally unstable with respect to both longitudinal and transverse perturbations. At this point, it remains to investigate the nature of the instabilities, so as to better understand the dynamics of this important class of solutions of the NLS equation.

Using Hill's method we numerically considered the instabilities due to transverse perturbations with wavenumber denoted by $\rho \in [0, 4]$. Note the $\rho = 0$ corresponds to one-dimensional, *i.e.* longitudinal, perturbations. For each NLS equation (*i.e.* for each choice of $\alpha, \beta = \pm 1$), and for each parameter pair (k, B), and for each perturbation of wave number ρ, a sequence of a sequence of Floquet parameters μ was chosen from the interval $[-\frac{\pi}{K}, \frac{\pi}{K}]$. The generalized eigenvalues and eigenvectors were computed from the resulting matrix. The eigenvalues are approximations of spectral elements of (8), and an approximation of the corresponding eigenfunctions may be reconstructed from the generalized eigenvectors.

Since a single eigenvalue with positive real part leads to instability of the system, the eigenvalue with largest real part over all choices of μ was recorded for each (k, B, ρ) triplet. That is, we compute

$$\Omega_{growth}(k, B, \rho) = \max_{\mu \in [-\pi/K, \pi/K]} Re\ \Omega(k, B, \rho, \mu), \tag{12}$$

which we call the growth rate for a given NTP solution with solution parameters (k, B) and perturbed with transverse wavenumber ρ. We reduce the dimension still further by computing the largest such growth rate over all sampled perturbation wavenumbers ρ. This quantity,

$$\Omega_{\max}(k, B) = \max_{\rho \in [0,4]} \Omega_{growth}(k, B, \rho), \tag{13}$$

the maximal growth rate over all ρ, is plotted in the first column of Figs. 2 and 3. This represents the maximal exponential growth rate that a solution with parameters (k, B) can undergo in the range examined, and allows us to determine the solution which is spectrally the most unstable. We also recorded the minimum growth rate over all ρ,

$$\Omega_{\min}(k, B) = \min_{\rho \in [0,4]} \Omega_{growth}(k, B, \rho), \tag{14}$$

to verify that all solutions are unstable with respect to every sampled perturbation.

Every point plotted in Figs. 2 and 3 corresponds to a solution, and the boundaries in the figure are the boundaries of the regions represented in Fig. 1 and correspond to limiting TP solutions. Fig. 2 corresponds to the x-focusing ($\alpha = 1$) parameter range $(k, B) = (0, 1) \times (2k^2, 2)$ in the $\alpha = 1$ case of Fig. 1(a). The one-to-one transform $T_f(B) = (B - 2k^2)/(2 - 2k^2)$ is used to normalize the range of B. This maps the interval $[2k^2, 2]$ to $[0, 1]$. Fig. 3 corresponds to the x-defocusing ($\alpha = -1$) parameter range of $(k, B) = (0, 1) \times (-1, 0)$ shown in Fig. 1(b). The transform $T_d(B) = -B$ is used in Fig. 3. A $\log_{10}$ scale is used in the vertical dimension of Figs. **??** and 3. This causes the panels of Fig. 2 to become increasing sparse in their lower right corners. The right-hand panels of Figs. 2 and 3 indicates the wavenumber ρ which leads to maximal growth shown in the left-hand panels. Recall that our computations were truncated at $\rho = 4$, and so in all cases maximums and minimums may occur at values of $\rho > 4$.

3.3.1 Case I: Elliptic setting with $\alpha = \beta = 1$ (Optics, BEC)

Panels Ia and Ib of Fig. 2 summarize some properties of the computed instabilities in the case of focusing in both the x- and y-dimensions. The lower boundary of the plot corresponds to $B = 2k^2 + (10^{-8})$, and so is only slightly away (in the parameter space of B) from a cn-type solution. The upper boundary is close to dn-type solutions, with $B = 1.99$. The left boundary of the plots, where $k = 0.01$, represents a region in parameter space near to Stokes' wave solutions. The entire right-hand boundary, where $k = 0.99$, is near to the bright soliton limit case which occurs at $(k, B) = (1, 2)$.

A distinct ridge of large instability is noticeable in the plot of $\Omega_{\max}$ in panel Ia of Fig. 2. The ridge appears to begin near the zero solution at $(k, B) = (0, 0)$, and remains close to the cn limit boundary (within approximately .02 units) as k increases. It reaches a global maximum of $R_{\max} = 5.666$ around $k = 0.96$. Moving away from the cn boundary results in the rapid increase of $\Omega_{\max}$. Movement away from the dn boundary results in a much slower increase in the value of $\Omega_{\max}$, as does moving away from the Stokes' wave boundary for B larger than approximately 0.001. The maximum value of $\Omega_{\max}$ over the sampled (k, B) space, given by $R_{\max} = 5.666$, is reached near $(k, B) \approx (0.99, 1.98)$. The minimum ($R_{\min} = 0.015693$) occurs near to $(k, B) \approx (0.01, 0.01)$ for $\rho = 4$.

In Ib, the wavelength corresponding to the maximal growth of Ia is given. In this case, the maximum instability occurs for the shortest wavelength samples, $\rho = 4$. This indicates that there is a strong short-wavelength (large ρ, possible infinite) instability.

3.3.2 Case II: Hyperbolic setting with $\alpha = -\beta = 1$ (Deep water waves)

Panels IIa and IIb of Fig. 2 summarize some properties of the computed instabilities in the case of focusing in the x-dimension and defocusing in the y-dimension. The lower boundary of the plot corresponds to $B = 2k^2 + (10^{-8})$, and so is just slightly away (in parameter space of B) from a cn-type solution. The upper boundary is close to dn-type solution, with $B = 1.99$. The left boundary of the plots, where $k = 0.01$, represents a region in parameter space near to Stokes wave solutions, while $k = 0.99$ on the left boundary. The bright soliton solution is the limiting case result when $k \to 1$.

As in Case I, a ridge of large instability is noticeable in the growth plot IIa. The ridge appears to begin near the zero solution at $(k, B) = (0, 0)$, and remains close to the cn-type limit boundary (within approximately .02 units) as k increases. This ridge has a local minimum near $k = 0.7$ and

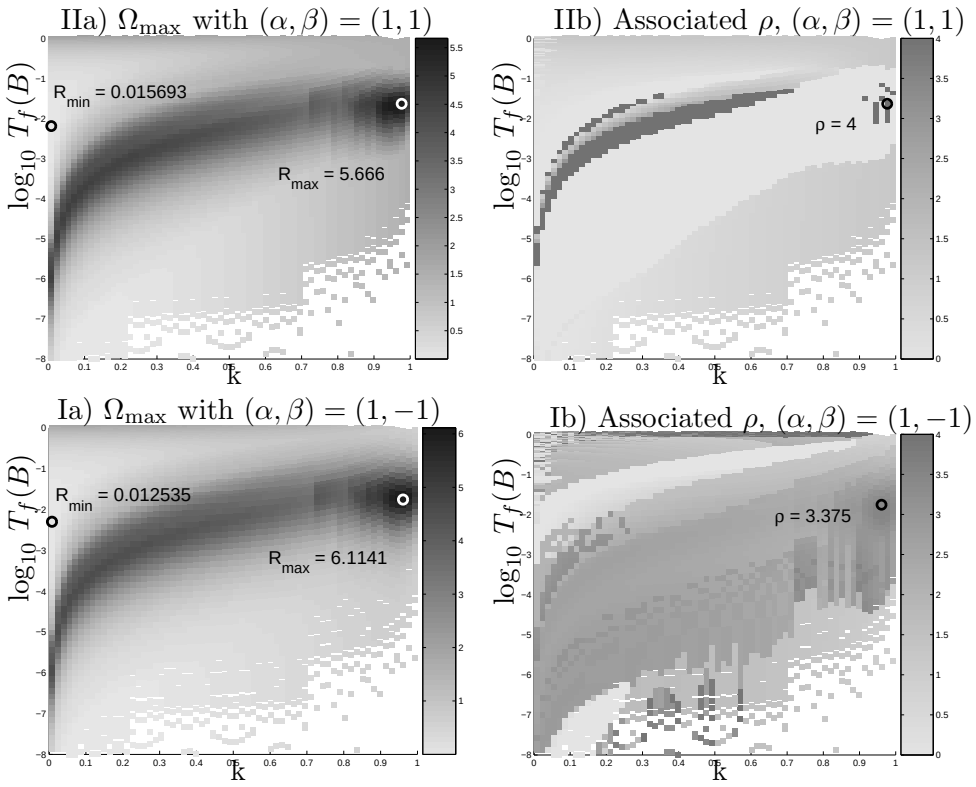

Figure 2: Focusing in x-dimension plots representing a) $\Omega_{\max}$ and b) the wavenumber ρ associated to $\Omega_{\max}$. $\mathrm{R}_{\max} = \max_{k,B} \Omega_{\max}$ and $\mathrm{R}_{\min} = \min_{k,B} \Omega_{\min}$. The vertical direction indicates the amount of nontrivial-phase in the underlying solution, and is plotted on a $\log_{10}$ scale. White space corresponds to (k, B)-parameter space that was *not* sampled.

increases again to a global (over all admissible (k, B)-parameter space) maximum near $k = 0.96$. As in the setting above, moving away from the cn-type boundary results in a rapid increase of $\Omega_{\max}$. Moving away from the dn boundary results in a much slower increase in the value of $\Omega_{\max}$. For $B > 0.001$, moving away from the boundary result in a similar slow increase in $\Omega_{\max}$. The maximum ($R_{\max} = 6.1141$) and minimum ($R_{\min} = 0.012535$) growth rates span a slightly larger range than the similar values in Fig. 2. These are centered near $(k, B) = (0.01, 0.01)$ and $(k, B) = (0.96, 1.98)$, respectively.

In IIb, the wavelength corresponding to the maximal growth $R_{\max}$ of IIa are given. In this case, the maximum instability of R_{max} occurs for $\rho = 3.375$. The surface represented by IIb appears to be much smoother than the surface of Ib.

3.3.3 Case III: Hyperbolic setting with $-\alpha = \beta = 1$ (Deep water waves)

Panels IIIa and IIIb of Fig. 3 summarize some properties of the computed instabilities in the case of defocusing in the x-dimension and focusing y-dimension. The lower limit of the plot corresponds to $B = -(10^{-8})$, and so is just slightly away from the sn-type solution. The left boundary of the plots, where $k = 0.01$, represents a region in parameter space near to Stokes wave solutions, while $k = 0.99$ on the left boundary. In the limit as $k \to 1$, the solution becomes a gray soliton.

A distinct ridge of large instability is noticeable in the growth plot IIIa. The ridge appears to begin near the zero solution limit at $(k, B) = (0, 0)$, and remains close to the sn limit boundary (within approximately .02 units) as k increases. It quickly reaches the global maximum (over all admissible (k, B)-parameter space) of $R_{\max} = 7.6375$ near $k = 0.02$ and $B = -0.0001$. The ridge then appears to decrease in amplitude as k increases towards 1. Moving away from the sn-type boundary results in a rapid increase of $\Omega_{\max}$. Moving away from the dn-type boundary results in a much slower increase in the value of $\Omega_{\max}$. Similarly, there is much slower increase when moving away from the Stokes' wave limit for $B > 0.001$. The maximum exponential growth rate, $R_{\max} = 7.6375$, occurs for $(k, B) \approx (0.02, 0.00001)$. The minimum exponential growth, $R_{\min} = 0.015578$ is found near $(k, B) \approx (0.01, 0.9)$. Both the maximum and minimum are located near to the Stokes' wave boundary.

The plot IIIa indicates short wave perturbations lead to large values of $\Omega_{\max}$. The largest growth occurs for a perturbation with wavenumber of $\rho = 3.625$.

3.3.4 Case IV: Elliptic setting with $-\alpha = -\beta = 1$ (Optics, BEC)

Panels IVa and IVb of Fig. 3 summarize some properties of the computed instabilities in the case of defocusing in both the x- and y-dimensions. The lower limit of the plot corresponds to $B = -(10^{-8})$, and so is just slightly away from the sn solution, as measured in the parameter B. The left boundary of the plots, where $k = 0.01$, represents a region in parameter space near to the Stokes wave solutions, while $k = 0.99$ on the left boundary. In the limit as $k \to 1$, the solutions become gray solitons.

A distinct ridge of large instability is noticeable in the growth plot IVa. The ridge appears to begin near the trivial limit $k = 0$ and $B = 0$, and remains close to the sn limit boundary (within approximately .02 units) as k increases, to reach a global maximum near $k = 0.02$ and $B = -0.0001$. The ridge then appears to decrease in amplitude as k increases towards 1. As in the setting above, moving away from the sn-type boundary results in a rapid increase of $\Omega_{\max}$. Moving away from the dn-type boundary results in a much slower increase in the value of $\Omega_{\max}$. The same is true when moving away from the Stokes boundary, when B is larger than approximately 0.001. The maximum exponential growth rate, $R_{\max} = 7.6456$, and the minimum, $R_{\min} = 0.0001556$, span a slightly larger range of values than do the values of $\Omega_{\max}$ in the panel above it. The maximum and minimum values are obtained near $(k, B) \approx (0.01, 0.00009)$ and $(k, B) \approx (0.01, -1)$, respectively. Both are located near to the Stokes' wave boundary.

In the plot IVb, wavenumbers corresponding to $\Omega_{\max}$ of IVa are given. It appears that a majority of the large values of $\Omega_{\max}$ are attributable to small ρ (long wave) perturbations. In fact, the largest growth occurs for $\rho = 0$, the one-dimensional perturbation. In contrast, short wavelength two-dimensional perturbations with wavenumber $\rho > 3$ were associated with many of the large $\Omega_{\max}$ values in the previous plots.

4 Summary

In this paper, we have considered the spectral instability of one-dimensional traveling-wave NTP solutions of the cubic nonlinear Schrödinger equation. Such solutions can be expressed in terms of Jacobi elliptic functions. An exact spectral form of the linearized operator is truncated and used to construct an associated generalized eigenvalue problem. The positive real part of the resulting

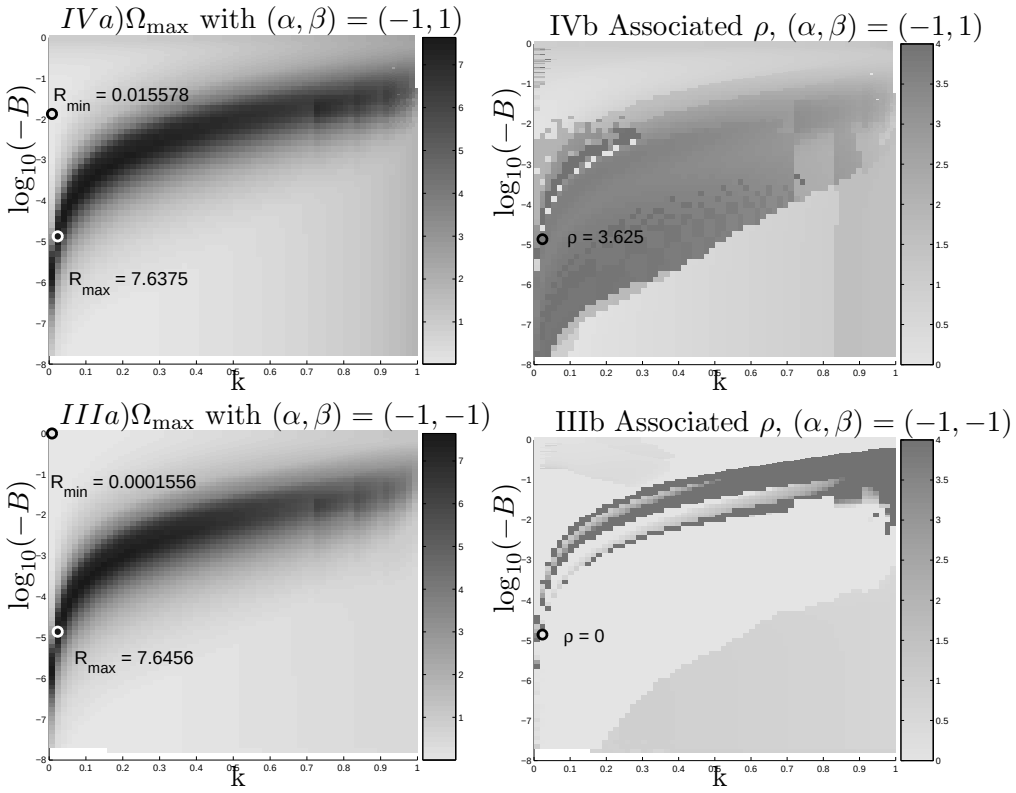

Figure 3: Defocusing in the x-dimension plots where a) is $\Omega_{\max}$ and b) the wavenumber ρ associated with $\Omega_{\max}$. $\mathrm{R}_{\max} = \max_{k,B} \Omega_{\max}$ and $\mathrm{R}_{\min} = \min_{k,B} \Omega_{\min}$. The vertical direction indicates the amount of nontrivial-phase in the underlying solution, and is plotted on a $\log_{10}$ scale.

eigenvalues was used to determine that there are *no* spectrally stable NTP solutions. The numerics indicate a well-defined ridge of maximal instability which is located in the (k, B)-parameter region associated with fully nontrivial-phase solutions. In addition, the numerical evidence indicates that exponential growth rates of dn-type solutions, and to a lesser extent the Stokes' wave solutions, are insensitive to transverse perturbation. The growth of the cn-type and sn-type solutions appear to be quite sensitive to this perturbation. In summary, numerical evidence suggests that bounded, nontrivial-phase one-dimensional traveling-wave solutions to the cubic NLS equation are unstable with respect to both one-dimensional and transverse perturbation.

References

[1] V. A. Aleshkevich, A. A. Egorov, Y. V. Kartashov, V. A. Vysloukh, and A. S. Zelenina. Stability of spatiotemporal cnoidal waves in cubic nonlinear media. *Phys. Rev. E*, 67:066605, 2003.

[2] P. F. Byrd and M. D. Friedman. *Handbook of Elliptic Integrals for Engineers and Physicists.* Springer-Verlag, Berline, 1954.

[3] L. D. Carr, C. W. Clark, and W. P. Reinhardt. Stationary solutions of the one-dimensional nonlinear Schrödinger equation. I. Case of repulsive nonlinearity. *Phys. Rev.A*, 62:63610, 2000.

[4] J. D. Carter and B. Deconinck. Stability of trivial-phase solutions of the two-dimensional cubic nonlinear Schrödinger equation. *Submitted for publication*, 2005.

[5] J. D. Carter and H. Segur. Instability in the two-dimensional cubic nonlinear Schrödinger equation. *Phys. Rev. E.*, 68(4):045601, 2003.

[6] B. Deconinck and J. N. Kutz. Computing spectra of linear operators using Hill's method. *Submitted for publication*, 2005.

[7] B. Deconinck, D. E. Pelinovsky, and J. Carter. Transverse instabilities of deep-water solitary waves. *Submitted for publication*, 2005.

[8] S. E. Fil'chenkov, G. M. Fraiman, and A. D. Yunakovskii. Instability of periodic solutions of the nonlinear Schrödinger equation. *Sov. J. Plasma Phys.*, 18(8):961–966, 1987.

[9] G. H. Golub and C. F. V. Loan. *Matrix Computations.* Johns Hopkins University Press, Baltimore, MD, 1996.

[10] E. Infeld and J. Ziemkiewicz. Stability of complex solutions of the nonlinear Schrödinger equation. *Acta Phys. Pol.*, A59(3):255–275, 1981.

[11] C. Jacobi. *Gessammel Werke.* Königsberg, 1829.

[12] Y. V. Kartashov, V. Aleshkevich, V. Vysloukh, A. Egorov, and A. Zelenina. Transverse modulational instability of (2+1)-dimensional cnoidal waves in media with cubic nonlinearity. *J. Opt. Soc. Am. B.*, 20(6):1273–1284, 2003.

[13] Y. S. Kivshar and D. E. Pelinovsky. Self-focusing and transverse instabilities of solitary waves. *Phys. Rep.*, 331(4):118–195, 2000.

[14] E. Kuznetsov, A. Rubenchik, and V. Zakharov. Soliton stability in plasmas and hydrodynamics. *Phys. Rep.*, 142:103–165, 1986.

[15] D. U. Martin, H. C. Yuen, and P. G. Saffman. Stability of plane wave solutions of the two-space-dimensional nonlinear Schrödinger equation. *Wave Motion*, 2:215–229, 1980.

[16] K. Rypdal and J. J. Rasmussen. Stability of solitary structures in the nonlinear Schrödinger equation. *Phys. Scripta*, 40:192, 1989.

[17] P. L. Sulem and C. Sulem. *Nonlinear Schrödinger Equations: Self-focusing and Wave Collapse.* Springer-Verlag, New York, NY, 1999.

[18] V. E. Zakharov and A. M. Rubenchik. Instability of waveguides and soliton in nonlinear media. *Sov. Phys. JETP*, 38(3):494–500, 1974.